IOP Conf. Series: Materials Science and Engineering **317** (2018) 012074 doi:10.1088/1757-899X/317/1/012074

Effects of the TiC Nanoparticle on Microstructures and Tensile Properties of Selective Laser Melted IN718/TiC Nanocomposites

Xiling Yao[1], Seung Ki Moon[1], Bing Yang Lee[2], Guijun Bi[2]

[1]Singapore Centre for 3D Printing, School of Mechanical & Aerospace Engineering, Nanyang Technological University, Singapore, 639798
[2]Singapore Institute of Manufacturing Technology Singapore 638075

Abstract. The purpose of this paper is to investigate the effects of TiC nanoparticle content on microstructures and tensile properties of the IN718/TiC nanocomposites fabricated by selective laser melting (SLM). 0.5wt%, 1.0wt%, and 2.0wt% of TiC nanoparticles are added to the IN718 powders. The bulk-form IN718/TiC nanocomposites with different TiC contents are fabricated in-situ by SLM using the same process settings. The evolution of microstructures and tensile properties as the effect of changing the TiC content is studied using the optical microscopy, scanning electron microscopy, X-ray diffraction analysis, and tensile testing. The increase of TiC content refines the microstructure, promotes the formation of the cellular morphology, and reduces the size and continuity of Laves precipitates. Increasing the TiC content improves the yield strength and ultimate tensile strength but decreases the ductility. The grain refinement, dislocation bowing, dislocation punching, and the reduction in Laves precipitate contribute to the strengthening effect in the IN718/TiC nanocomposites.

1. Introduction

Selective laser melting (SLM) is one of the “Power Bed Fusion” additive manufacturing (AM) processes for fabricating metallic parts. In the SLM process, metal powders are rapidly melted by a high-energy laser and then re-solidify to form metallurgical bonding [1]. SLM has been used to fabricate bulk-form parts in many different metallic materials, including titanium [2], aluminum [3], iron [4], cobalt-chrome [5], and nickel alloys [6]. The directional solidification and the rapid cooling rate (106-7K/s) generate unique microstructures for selected laser melted metals, including highly-oriented dendrites and ultra-fine grains, which result in different (sometimes superior) mechanical properties compared with cast and wrought metals [7-9].

Among Ni-based superalloys, IN718 is a Ni-Fe-Cr austenitic (γ) superalloy with good weldability [10]. IN718 have found broad applications in gas turbines and petrochemical equipment, due to its superiority in both strength and temperature properties [11]. IN718 has been manufactured by the SLM process successfully in previous research [12-15]. In as-built IN718 via SLM, the growth of γ' and γ'' precipitates is inhibited by the rapid solidification rate, while the γ matrix and Laves precipitates are the major constituent phases [16]. IN718 fabricated by SLM displays dendritic microstructures, which undergo morphological changes at different laser energy density [14]. Compared with the cast material, the enhanced hardness, wear performance, and oxidation resistance was observed in the SLM-fabricated IN718 due to microstructure refinement [15].

Content from this work may be used under the terms of the Creative Commons Attribution 3.0 licence. Any further distribution of this work must maintain attribution to the author(s) and the title of the work, journal citation and DOI.
Published under licence by IOP Publishing Ltd

Ceramic particle reinforced MMCs are important materials in engineering applications due to their superior properties such as high strength and wear resistance. Ni-based MMCs reinforced by different types of ceramic particles were fabricated by laser-powered AM processes, during which the unmolten ceramic particles were embedded in metal matrices upon melt pool solidification. Cooper et al. [17] mixed Al2O3, SiC, and TiC micro-sized particles with IN625 powders and fabricated the MMCs using additive layer manufacturing (ALM). Improved hardness was observed in SiC and TiC reinforced MMCs compared with the pure IN625. In a similar research [18], micro-sized TiC particles were added to IN718, and the MMC was fabricated by laser metal deposition (LMD). The microhardness and wear properties were improved by increasing the input laser energy density. Jia and Gu [19] applied the SLM process to fabricated IN718-based MMC reinforced by TiC nanoparticles. The effects of laser energy on the density, microhardness, and wear rate of the IN718/TiC nanocomposite were studied.

In this paper, fully-dense IN718/TiC nanocomposites were fabricated in-situ by the SLM process. Different weight percentages (i.e. 0.5%, 1.0% and 2.0%) of TiC nanoparticles were used, and the evolution of microstructures and tensile properties as the effect of changing the TiC nanoparticle content was investigated. Optical microscopy (OM), scanning electron microscopy (SEM), and X-ray diffraction (XRD) were applied to analyse the microstructural morphologies and crystal phases. Strengthening mechanisms in the SLM-fabricated IN718/TiC nanocomposites were also discussed.

2. Experimental Setup

2.1. Powder Preparation

Gas atomized spherical IN718 powders were used as the matrix material in the selective laser melted nanocomposites. The powder diameters ranged from 21 to 55μm. The chemical compositions of the IN718 powders are listed in table 1. Spherical TiC nanoparticles had diameters ranging from 80 to 150 nm. Three levels of TiC nanoparticle content in weight percentage, i.e. 0.5 wt%, 1.0 wt%, and 2.0wt%, were added to the IN718 powders. The IN718/TiC mixtures in powder form were then blended in an Inversina Tumbler Mixer (Bioengineering, Inc.) at 70rpm for 8 hours before being loaded into the SLM machine as the build material.

Table 1. Chemical compositions of the IN718 powders.

Element	**Ni**	**Cr**	**Nb**	**Mo**	**Co**	**Ti**
wt%	50-55	17 -21	4.75-5.5	2.8-3.3	1.0	0.65-1.15
Element	**Mn**	**Si**	**Al**	**Cu**	**Fe**	
wt%	0.35	0.35	0.2-0.8	0.3	Bal	

2.2. Selective Laser Melting Process

Sample fabrications were performed in an SLM 250HL machine manufactured by SLM Solutions GmbH. The SLM machine utilizes a ytterbium fiber laser with a wavelength of 1070nm and the maximum power of 300W. Argon gas was purged in the build chamber, and the oxygen level was reduced to 0.05% or lower during the process. Carbon steel plates are used as substrates, which were pre-heated to 100°C before the laser was activated in order to reduce the thermal stress at the substrate/part interface. During the SLM process, the laser scanned on the powders over the area where the part was being built. The hatch orientation rotated 79 degrees every layer to relieve the residual stress. As-fabricated parts were separated from the substrate via wire cutting at room temperature.

Table 2. SLM process parameters for specimen fabrication.

Laser power	**Layer thickness**	**Scan speed**	**Hatch space**
300 W	0.05 mm	800 mm/s	0.13 mm

Preliminary tests were conducted to identify the suitable SLM process parameters for producing fully dense parts in pure IN718 and IN718/TiC nanocomposites. The identified SLM process

parameters are listed in table 2. The same set of parameters was used to fabricate all specimens for material characterizations described in the rest of this paper.

2.3. Material Characterizations

Crystal phases were identified by X-ray diffraction (XRD) (D8 Discover, Bruker) with Cu Kα radiation (40 kV, 40 mA). X-ray scanning was from 30° to 95° with the step size of 0.05°. Specimens are polished down to 0.05μm finish. To reveal the microstructures, polished samples are electro-etched in 70% phosphoric acid at 10V for 15 seconds. Microstructures were observed using optical microscopy (OM, OLYMPUS MX51) and scanning electron microscopy (SEM; ZEISS EVO 50). Tensile coupons following the ASTM E8 standard were machined from SLM fabricated rectangular blocks by wire cutting, as shown in figure 1. The loading orientations of the tensile coupons were perpendicular to the SLM build direction (Z-axis) and parallel to the X-Y plane. Tensile tests were conducted using an Instron Universal Tester at room temperature. Yield strength (YS), ultimate tensile strength (UTS), and percentage elongation at fracture were obtained from the tensile testing results. Fracture surfaces of the broken tensile coupons were observed using the SEM.

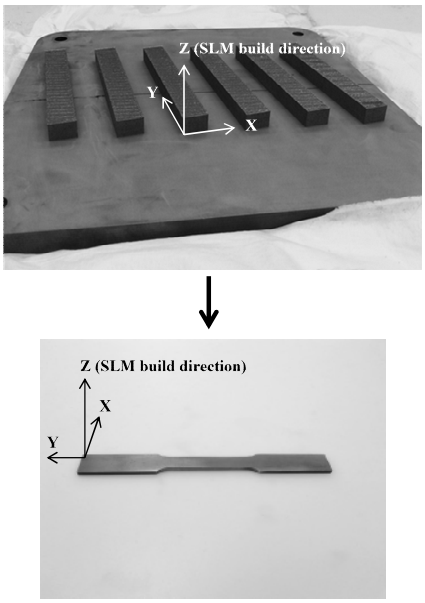

Figure 1. Tensile coupons machined from the SLM-fabricated rectangular blocks.

3. Results and Discussion

Bulk-form samples in pure IN718 and IN718/TiC nanocomposites with three different TiC nanoparticle contents (0.5, 1.0, and 2.0wt%) are fabricated from the powders by SLM. Densities of the specimens are measured to be higher than 99.9% of the theoretical values. The as-built samples display good surface finish and clear surface design features (i.e. the indented characters created in the CAD models). Cracks and distortions are absent.

3.1. Microstructures

OM images taken from IN718/TiC nanocomposites with different TiC contents are shown in figure 2. Cumulatively-stacked scale-like melt pools are observed on the vertical plane parallel to the build direction (+Z). The concave shapes of the melt pools are formed by the Gaussian laser input in SLM. Small amounts of micro-sized pores caused by entrapped air bubbles appear at melt pool boundaries, which can hardly be avoided completely in SLM due to fast solidification.

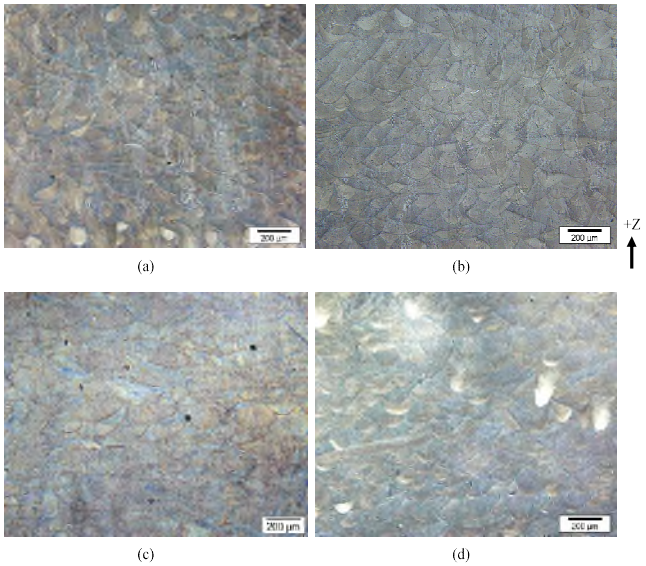

Figure 2. OM images of the (a) pure IN718, (b) IN718/0.5%TiC, (c) IN718/1.0%TiC, and (d) IN718/2.0%TiC nanocomposites.

Microstructure morphologies of pure IN718 and IN718/TiC nanocomposites with different TiC contents are shown in the SEM images (figure 3). Columnar microstructures oriented along the build direction are dominating in the SLM-fabricated pure IN718. The parallel dendritic grains with the spacing of about 2-3μm are formed by the highly directional cooling during the SLM process. The laser-induced heat flux in the melt pool orients vertically upwards, due to the vertical temperature gradient between the previously solidified layers and the current molten layer. With the addition of TiC nanoparticles, the SLM-fabricated IN718/TiC nanocomposites display a characteristic morphology dominated by equiaxed cellular microstructures with small cell aspect ratios. Long columnar grains still exist in IN718/TiC nanocomposites, but with decreased amount and size. In addition, finer microstructures are observed in the SLM-fabricated IN718/TiC nanocomposites compared with the pure IN718.

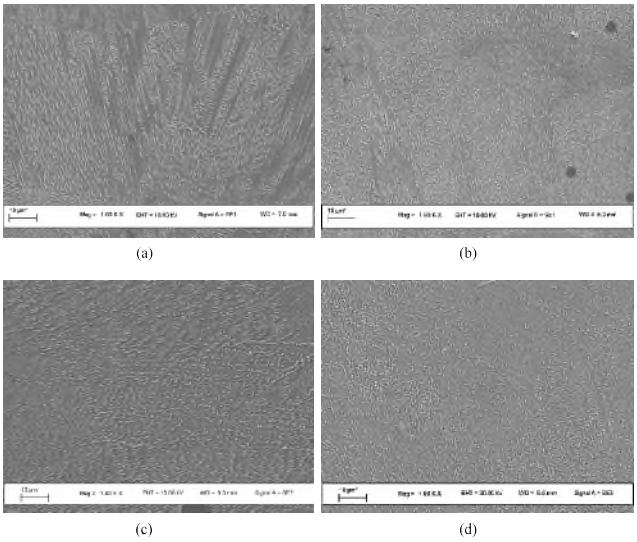

Figure 3. Low magnification SEM images of the (a) pure IN718, (b) IN718/0.5%TiC, (c) IN718/1.0%TiC, and (d) IN718/2.0%TiC nanocomposites

High magnification SEM images of the SLM-fabricated pure IN718 and IN718/TiC nanocomposites are shown in figure 4. The microstructure morphology of IN718/TiC nanocomposites varies with the TiC nanoparticle content. As the TiC content increase from 0 to 2.0%, the cell spacing decreases. As shown in figure 4, in the melt pool of the SLM-fabricated pure IN718, the solidification directions start from the melt pool boundary towards the center, being aligned with the thermal gradients caused by the Gaussian laser. In the IN718/TiC nanocomposites, as unmolten TiC nanoparticles are dispersed in the melt pool, they act as additional nucleation sites during crystallization and inhibit the grain growth. The higher solidification rate around the TiC nanoparticles contributes to the formation of finer microstructures in IN718/TiC nanocomposites [20]. The microstructure refinement effect of nanoparticles was also found in arc-welded materials [21].

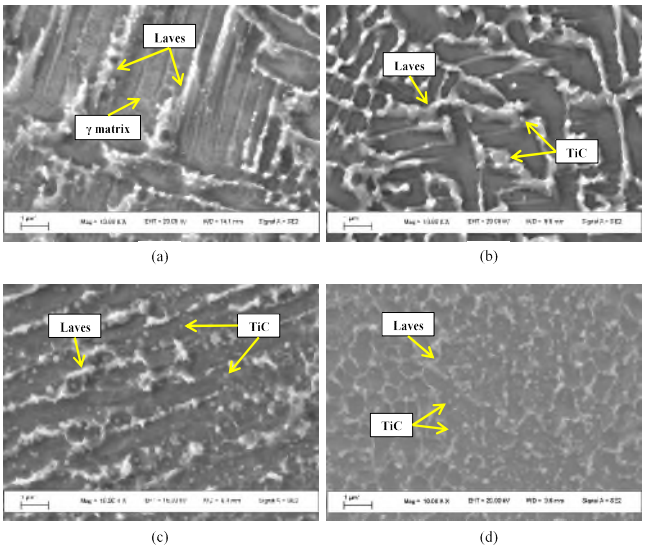

Figure 4. High magnification SEM images of the (a) pure IN718, (b) IN718/0.5%TiC, (c) IN718/1.0%TiC, and (d) IN718/2.0%TiC nanocomposites

The γ (fcc Ni-Fe-Cr) matrix and Laves (TCP, (Ni, Fe, Cr)2(Nb, Mo, Ti)) intermetallic compounds are the major constituents of the SLM-fabricated pure IN718 and IN718/TiC nanocomposites. Large and continuous Laves precipitates are observed in the pure IN718. As the TiC nanoparticle content increases in the IN718/TiC nanocomposites from 0.5 to 2.0%, the continuity of Laves gradually breaks down while the precipitates' size decreases. The formation of smaller and discontinuous precipitates in the IN718/TiC nanocomposites is caused by their higher solidification rates that cause insufficient Nb segregation [22]. Al, Ti, and Nb-rich precipitates such as the δ (orthorhombic Ni3Nb) phase and MC/M23C6/M6C carbides are not visible in the SEM images of the SLM-fabricated pure IN718 and IN718/TiC nanocomposites, due to inhibited atom (Al, Ti, Nb) segregation.

As shown in figures 4 (b), (c), and (d), spherical TiC nanoparticles (80-100nm diameter) are dispersed in the γ matrix of the IN718/TiC nanocomposites. Agglomeration of TiC nanoparticles has not occurred due to the high laser energy density (375J/m), calculated as the ratio of the laser power to scan speed. The high laser energy density results in intense Marangoni convection, low viscosity of the molten metal, and long circulating time for unmolten nanoparticles in the melt pool [23]. The avoidance of nanoparticle agglomerations reduces the detrimental micro-cracks formation in the matrix and hence prevents the deterioration of mechanical properties.

XRD analysis was carried out to identify crystal structures in the SLM-fabricated pure IN718 and IN718/TiC nanocomposites, as shown in the XRD spectra in figure 5. The γ crystal phase is found based on the ICDD database (PDF Number 00-035-1375, Ni-Cr-Fe). As the TiC nanoparticle content increases from 0 to 2.0%, no new peaks in the XRD spectra appear. Diffraction peaks corresponding to TiC cannot be seen, due to the small size of TiC nanoparticles in the matrix. Other crystal structures such as δ and MC carbides are not detected, indicating no or very little phase transition during the

SLM process. The strongest (200) peak in the pure IN718 indicates a preferable crystal orientation along the build direction as a result of laser-induced directional solidification (Amato et al. 2012). The prominence of the (200) peak remains in the IN718/0.5%TiC nanocomposite. However, as the TiC nanoparticle content increase to 1.0 and 2.0%, the (200) peak becomes weaker and it is no longer the most dominating peak. This change indicates a slightly more random distribution of crystal orientations in the IN718/TiC nanocomposites than in the pure IN718.

3.2. Tensile Properties

As the result of the tensile test, the tensile properties of the SLM-fabricated pure IN718 and IN718/TiC nanocomposites with different TiC contents are listed in table 3. The characteristic tensile stress-strain curves of these materials are compared in figure 6. It can be observed that the SLM-fabricated IN718/TiC nanocomposites have higher yield strength (YS) and ultimate tensile strength (UTS) but lower elongate at fracture than the pure IN718. As the TiC nanoparticle content in the IN718/TiC nanocomposites increases from 0.5 to 2.0%, both YS and UTS improved while the elongation decreases.

The large and continuous Laves precipitates in the SLM-fabricated pure IN718 is detrimental to the material's strength. By increasing the fraction of TiC nanoparticles, the amount of Laves precipitates is decreased in the IN718/TiC nanocomposites. Therefore, the IN718/TiC nanocomposites suffer less from the weakening effect of Laves precipitates compared with the pure IN718.

As a trade-off of the strengthening effect of TiC nanoparticles in enhancing YS and UTS, the elongation at fracture decreases when the TiC content increases from 0 to 2.0%. After the tensile stress-strain exceeds the yield point, the matrix-TiC interfaces act as failure initiators where cracks may form and grow. Therefore, the addition of TiC nanoparticles increases the number of failure initiating sites after yielding and hence brings the final fracture earlier than the pure IN718.

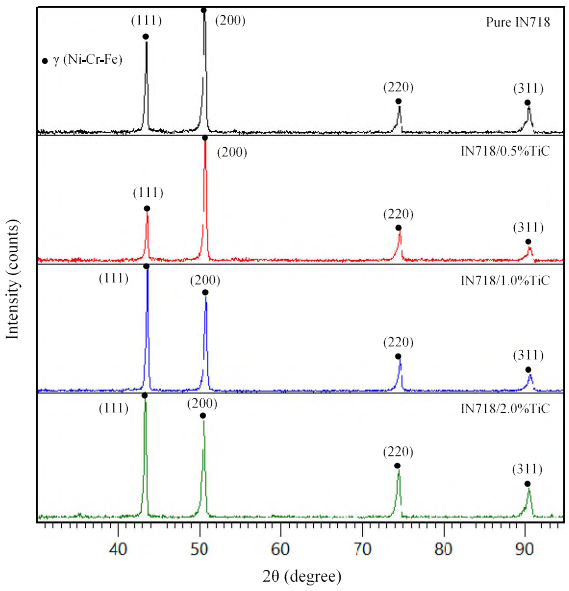

Figure 5. XRD spectra of the SLM-fabricated pure IN718 and IN718/TiC nanocomposites.

Table 3. Tensile properties of the SLM-fabricated pure IN718 and IN718/TiC nanocomposites.

Materials	YS (MPa)	UTS (MPa)	Elongation (%)
Pure IN718	638.6	933.6	38.29
IN718/0.5%TiC	674.1	947.7	29.20
IN718/1.0%TiC	709.3	1023.0	17.27
IN718/2.0%TiC	800.7	1068.0	13.91

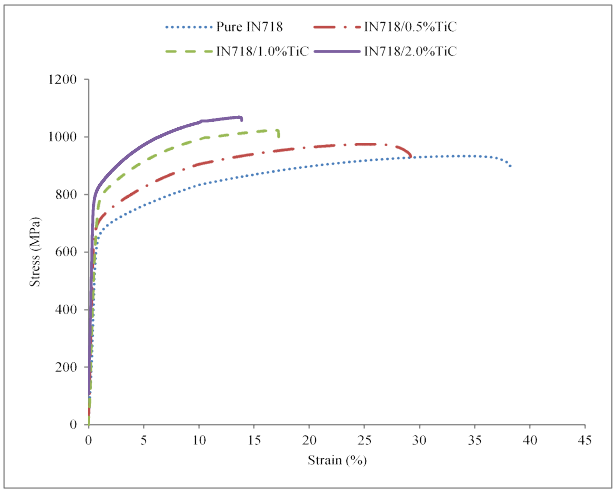

Figure 6. Tensile stress-strain curves of the SLM-fabricated pure IN718 and IN718/TiC nanocomposites

4. Conclusions

In this research, the SLM process was applied to fabricate IN718/TiC nanocomposites with different weight percentages (0, 0.5%, 1.0%, and 2.0%) of TiC nanoparticle. The effects of the TiC content on microstructures and the tensile properties of the SLM-fabricated IN718/TiC nanocomposites were investigated, and the findings are summarized as below:

1) Fully-dense specimens in the pure IN718 and IN718/TiC nanocomposite with different TiC contents can be fabricated using the same set of SLM process parameters. Surface defects or geometric distortions are absent.

2) Compared with the dominating columnar grains in the SLM-fabricated pure IN718, the microstructures of the IN718/TiC nanocomposites display finer cellular morphologies, and the cell spacing decreases with the increasing TiC nanoparticle content.

3) Compared with the large and continuous Laves precipitates in the SLM-fabricated pure IN718, the Laves precipitates decrease in size while the continuity breaks down as the TiC content increases in the IN718/TiC nanocomposites, due to higher solidification rate.

4) The increment of the TiC content from 0 to 2.0wt% increases both the yield strength and ultimate tensile strength but decreases the elongation at fracture.

In future research, the SLM process can be applied to fabricated IN718-based metal matrix composites with other reinforcements, such as oxides, borides, and carbon nanotubes (CNT). Apart from mechanical properties, thermal and chemical properties of SLM-fabricated IN718-based MMCs can also be studied in the future.

References

[1] Kruth J P, Mercelis P, Vaerenbergh J V, Froyen L, and Rombouts M 2005 *Rapid Prototyp. J.* **11(1)** 26-36.
[2] Pawlak A, Szymczyk P, Ziolkowski G, Chlebus E and Dybala B 2015 *Rapid Prototyp. J.* **21(4)** 393-401.
[3] Kempen K, Thijs L, Van Humbeeck J and Kruth J P 2012 *Phys. Proc.* **39** 439-46.
[4] Song B, Dong S, Deng S, Liao H and Coddet C 2014 *Opt. Laser Tech.* **56** 451-60.
[5] Vandenbroucke B and Kruth J P 2007 *Rapid Prototyp. J.* **13(4)** 196-203.
[6] Carter L N, Essa K and Attallah M M 2015 *Rapid Prototyp. J.* **21(4)** 423-32.
[7] Brandl E, Heckenberger U, Holzinger V and Buchbinder D 2012 *Mater. Des.* **34** 159-69.
[8] Liu Z H, Zhang D Q, Sing S L, Chua C K and Loh L E 2014 *Mater. Charact.* **94** 116-25.
[9] Thijs L, Kempen K, Kruth J P and Van Humbeeck J 2013 *Acta. Mater.* **61(5)** 1809-19.

[10] Knorovsky G A, Cieslak M J, Headley T J, Romig A D and Hammetter W F 1989 *Metallurg. Trans. A* **20(10)** 2149-58.
[11] Zhang S and Zhao D 2012 *Aerospace Materials Handbook* CRC Press Boca Raton Florida US.
[12] Strößner J, Terock M and Glatzel U 2015 *Adv. Eng. Mater.* **17**(8) 1099-105.
[13] Amato K N, Gaytan S M, Murr L E, Martinez E, Shindo P W, Hernandez J, Collins S and Medina F 2012 *Acta. Mater.* **60(5)** 2229-39.
[14] Jia Q and Gu D 2014 *J. Alloy. Comp.* **585** 713-21.
[15] Jia Q and Gu D 2014 *Opt. Laser Tech.* **62** 161-71.
[16] Zhang D, Niu W, Cao X and Liu Z 2015 *Mater. Sci. Eng. A* **644** 32-40.
[17] Cooper D E, Blundell N, Maggs S and Gibbons G J 2013 *J. Mater. Proc. Tech.* **213(12)** 2191-200.
[18] Hong C, Gu D, Dai D, Gasser A, Weisheit A, Kelbassa I, Zhong M and Poprawe R *Opt. Laser Tech.* **54** 98-109.
[19] Jia Q and Gu D 2014 *J. Mater. Res.* **29(17)** 1960-9.
[20] Sing S L, Yeong W Y and Wiria F E 2016 *J. Alloy. Comp.* **660** 461-70.
[21] Fattahi M, Mohammady M, Sajjadi N, Honarmand M, Fattahi Y and Akhavan S 2015 *J. Mater. Proc. Tech.* **217** 21-9.
[22] Manikandan S G K, Sivakumar D, Rao K P and Kamaraj M 2014 J. Mater. Proc. Tech. **214(2)** 358-64.
[23] Yuan P, Gu D and Dai D 2015 Mater. Des. **82** 46-55.

Acknowledgment
This research was supported by SIMTech-NTU Joint Lab, National Research Foundation, Singapore, and Singapore Centre for 3D Printing.